Journal of Applied Physics ARTICLE scitation.org/journal/jap

Thermally corrected solutions of the one-dimensional wave equation for the laser-induced ultrasound

Cite as: J. Appl. Phys. **130**, 025104 (2021); doi: 10.1063/5.0050895
Submitted: 19 March 2021 · Accepted: 22 June 2021 ·
Published Online: 12 July 2021

Misael Ruiz-Veloz,[1] Geminiano Martínez-Ponce,[2] Rafael I. Fernández-Ayala,[1] Rigoberto Castro-Beltrán,[1] Luis Polo-Parada,[3] Bartolome Reyes-Ramírez,[2] and Gerardo Gutiérrez-Juárez[1,a)]

AFFILIATIONS

[1]División de Ciencias e Ingenierías, Universidad de Guanajuato, Loma del Bosque 103, Lomas del Campestre, C.P. 37150, León, Guanajuato, Mexico
[2]Centro de Investigaciones en Óptica A.C., Loma del Bosque 115, Lomas del Campestre, C.P. 37150, León, Guanajuato, Mexico
[3]Department of Medical Pharmacology and Physiology and Dalton Cardiovascular Research Center, University of Missouri-Columbia, 134 Research Park Drive Rd., Columbia, Missouri 65211, USA

[a)]**Author to whom correspondence should be addressed:** ggutj@fisica.ugto.mx. **URL:** www.fisica.ugto.mx/~ggutj

ABSTRACT

When thermal and stress confinement conditions are satisfied, the propagation of laser-induced ultrasound (LIU) is governed by an inhomogeneous wave equation for pressure, and the laser temporal profile can be modeled by a Dirac delta distribution. If these conditions are not fulfilled, the coupled differential equations for temperature and pressure must be solved, considering a laser pulse with finite time-width. Here, an exact solution of the boundary value problem for the 1D-wave equation is obtained in both the frequency domain and the time domain. Since highly absorbent optical materials are out of the validity range of the confinement conditions, these are used as a numerical and experimental model. It is shown that the impulse-response model correctly predicts the time of flight of photoacoustic waves. However, when considering a laser pulse with finite time-width, the resultant theoretical amplitude of the LIU signal decays rapidly to zero, which is not observed in the experiment. To overcome this, we propose a thermal correction on the LIU source, defined typically as the optical penetration length, which imposes a redefinition of stress and thermal confinement in just one statement. Additionally, with the aim of comparing the corrected-theoretical results with the acquired electrical signals, the sensor and the oscilloscope were modeled as an RC circuit in parallel. It was found that the amplitude of the electrical signal was proportional to the difference of the LIU amplitudes at the faces of the sensor. It is demonstrated that even though the sensor impulse response is modeled as a Dirac delta distribution, this difference strongly affects the shape of the LIU electrical signals, hiding relevant information of the acoustic waves.

I. INTRODUCTION

The transference of fluence in a short-time laser pulse to condensed matter brings about a transient non-radiative process that produces ultrasound stress waves in the surrounding medium. This phenomenon, known as laser-induced ultrasound (LIU) or pulsed photoacoustic (PA) effect, is ideal for locating and recognizing optical absorbers dispersed in biological tissue.[1–3] LIU stress waves, which propagate from the LIU source to the surrounding medium, are strongly dependent on the selected features of the excitation optical source and can be bulk stress waves (longitudinal and transversal) as well as Rayleigh and Lamb waves.[4] In the last decade, the interest in LIU has grown because it combines ultrasound high spatial resolution and weak scattering in deep imaging of biological tissues limited by optical diffusion.[5,6] These facts have caused that based LIU imaging can be considered as one of the most successful technological developments with applications in soft tissues, including detection of clinical metal implants such as coronary stents, needles, staples, and brachytherapy seeds.[7,8] Most of LIU imaging is based on the solution of an inhomogeneous wave equation with a Dirac delta distribution as a physical model for the laser temporal profile. In the case of a

metallic photoacoustic source, having a strong optical absorbance ($\sim 10^8$ m^{-1}), this model should not be used to describe the generation of photoacoustic waves because thermal and stress confinement conditions are not accomplished.

For the LIU phenomenon in liquid samples under the thermoelastic regime, it is well known and accepted that LIU has its theoretical foundations in the fluid theory.[9,10] Starting with the linearized equations of fluid dynamics, the generation and propagation of LIU is governed by the heat diffusion equation for temperature, $T(\mathbf{r}, t)$, coupled with the wave equation for pressure, $P(\mathbf{r}, t)$,[1,9–11]

$$\left(\frac{\partial}{\partial t} - \chi\nabla^2\right) T(\mathbf{r}, t) = \frac{1}{\rho_0 C_P} H(\mathbf{r}, t), \tag{1}$$

$$\left(\frac{\partial^2}{\partial t^2} - \frac{1}{K_T \rho_0}\nabla^2\right) P(\mathbf{r}, t) = \frac{\beta}{K_T}\frac{\partial^2}{\partial t^2} T(\mathbf{r}, t), \tag{2}$$

where χ is the thermal diffusivity, C_P is the heat capacity at constant pressure, β is the thermal expansion coefficient, K_T is the isothermal compressibility of the sample, and ρ_0 and T_0 are the mass density and temperature of the unperturbed medium, respectively.

In Eq. (1), $H(\mathbf{r}, t)$ is the density of electromagnetic energy per unit of time absorbed by the sample and has been modeled as $H(\mathbf{r}, t) = \mu(\mathbf{r}, t) I(\mathbf{r}, t)$, where $\mu(\mathbf{r}, t)$ is the sample optical absorption coefficient and $I(\mathbf{r}, t)$ is the laser fluence rate. The optical absorption coefficient can be time-dependent if, during experiments, photobleaching or photodamage is induced in the irradiated area.[12,13]

In order to decouple Eqs. (1) and (2), conventionally, two conditions have been proposed:

- **Thermal confinement:** *If* $\tau_{th} \gg \tau_p$, *the heat conduction can be neglected*,[2] *i.e.*, $\nabla T(\mathbf{r}, t) \approx \mathbf{0}$. Then, a combination of Eqs. (1) and (2) leads to the PA wave equation

$$\left(\nabla^2 - \frac{1}{c^2}\frac{\partial^2}{\partial t}\right) P(\mathbf{r}, t) = -\frac{\beta}{C_p} F(\mathbf{r}) \frac{\mathrm{d}\theta(t)}{\mathrm{d}t}, \tag{3}$$

  with τ_{th} as the heat diffusion time, τ_p the laser pulse time, and c as the speed of LIU in the fluid. Thermal confinement implies that the heating is only due to optical absorption and suggests that the heated volume cannot release its temperature excess throughout the excitation process.
- **Stress confinement:** *If* $\tau_{ac} \gg \tau_p$, *the stress confinement is achieved, and* $\theta(t)$ *can be approximated to a Dirac delta temporal function*, $\delta(t)$. τ_{ac} is the acoustic relaxation time, namely, the required time by the sample to expand over the illuminated region. It is defined as $\tau_{ac} = a/c$, where a is a characteristic length of heat.

For the one-dimensional approach, using a laser excitation beam with a large diameter, it is accepted that the characteristic length is the optical penetration depth, $a = 1/\mu$, and the heat diffusion time is equal to $1/4\chi\mu^2$.[14]

Even though the thermal and stress confinement conditions are not fulfilled for optical strongly absorbent materials, the wave equation has been used in the inverse problem for metals,[7,8] which suggests that it is possible to avoid solving the coupled Eqs. (1) and (2).

To obtain the LIU waveform after the absorption of an optical impulse, that is, the impulse response of the photoacoustic system, the 1D-wave equation has been solved in free space for samples that follow the Beer–Lambert law[15] as well as for optically thin samples ($\exp[-\mu(\mathbf{r})|z|] \approx 1$).[10] Accordingly, a more complete 1D-boundary value problem has been obtained in the case of plane samples surrounded by a transparent fluid, where a large acoustic impedance mismatch has been assumed.[16,17] It was shown that, in the time domain, LIU waveform is composed of a pressure peak followed by reflected and inverted pulses with a periodicity related to the sample's width and sound speed.[17] By using the Green method to solve this boundary value problem, an analysis in the frequency domain was done by Baddour and Mandelis.[18] Here, an experimental verification of the solution for infinite aluminum-samples also was done, assuming *a priori* the requirement of the thermal and stress confinement conditions.

In this paper, by Refs. 16–18, the 1-D wave equation boundary value problem is solved in frequency and time domains for laser pulses having both the Dirac delta and Gaussian time profiles. The sample was assumed to follow the Lambert–Beer law for optical absorption. As an experimental and numerical model, an aluminum slab was used. The numerical implementation of the obtained theoretical impulse-response solution matched well with the experimental time of flight results, although the stress confinement is not satisfied; on the other hand, for a Gaussian temporal profile, the numerical evaluation of the resultant theoretical pressure showed that the amplitude falls to zero, as it is expected because the thermal confinement is not satisfied. In order to overcome the discrepancy between theory and experiment, a heuristic correction is used. The correction is based on the thermal confinement condition and the fact that heat propagates a longer distance than the optical penetration depth during the illumination time. With this correction, the theoretical solutions of the wave equation, without the need of solving the coupled equations, do not vanish for the Gaussian pulse and predict accurately the time of flight of experimental results. To better compare the corrected-theoretical result with the measurement electrical signals, the sensor and the oscilloscope were modeled as a parallel RC circuit, it is found that LIU amplitudes are strongly affected by the measurement processes even though the sensor transfer function is modeled as a Dirac delta distribution.

II. THEORY

A. Frequency domain solution

For a plane sample s with thickness L, immerse on a non-optically absorbent fluid f, the 1D PA wave equation was solved, considering an electromagnetic pulse of fluence I_0 and with temporal profile $\theta(t)$, see the Appendix.

The solutions to the 1D PA wave equation in the temporal Fourier domain are

$$\hat{P}_B(z,\omega)=\overline{T}\frac{P_0}{2}\sum_{n=0}^{\infty}R^{2n}\left\{\left[\frac{e^{j\omega\left(\frac{z}{c_f}-2n\tau\right)}}{\omega_{ac}+j\omega}-e^{-\omega_{ac}\tau}\frac{e^{j\omega\left[\frac{z}{c_f}-(2n+1)\tau\right]}}{\omega_{ac}+j\omega}\right]\right.$$
$$\left.-R\left[\frac{e^{j\omega\left[\frac{z}{c_f}-2(n+1)\tau\right]}}{\omega_{ac}-j\omega}-e^{-\omega_{ac}\tau}\frac{e^{j\omega\left[\frac{z}{c_f}-(2n+1)\tau\right]}}{\omega_{ac}-j\omega}\right]\right\}\hat{\theta}(\omega),$$
$$z\le 0, \tag{4a}$$

$$\hat{P}_F(z,\omega)=\overline{T}\frac{P_0}{2}\sum_{n=0}^{\infty}R^{2n}\left\{\left[\frac{e^{-j\omega\left[\frac{z-L}{c_f}+(2n+1)\tau\right]}}{\omega_{ac}-j\omega}-e^{-\omega_{ac}\tau}\frac{e^{-j\omega\left[\frac{z-L}{c_f}+2n\tau\right]}}{\omega_{ac}-j\omega}\right]\right.$$
$$\left.-R\left[\frac{e^{-j\omega\left[\frac{z-L}{c_f}+(2n+1)\tau\right]}}{\omega_{ac}+j\omega}-e^{-\omega_{ac}\tau}\frac{e^{-j\omega\left[\frac{z-L}{c_f}+2(n+1)\tau\right]}}{\omega_{ac}+j\omega}\right]\right\}\hat{\theta}(\omega),$$
$$z\ge L, \tag{4b}$$

where subindexes B and F indicate the backward and forward propagated pressures, respectively. $P_0=\Gamma\mu I_0$ with $\Gamma\equiv c_s^2\beta/C_p$ are the initial pressure distribution and the Grüneisen parameter, respectively. $\tau=L/c_s$ is the single-trip time-of-flight of the acoustic wave in the slab and $\omega_{ac}\equiv\mu c_s$ the characteristic ultrasonic frequency of LIU. $R\equiv(Z_s-Z_f)/(Z_s+Z_f)$ is the acoustic reflectivity, where $Z_l\equiv c_l\rho_l$ with $l=\{f,s\}$ are the acoustic impedances for fluid and sample, respectively.

B. Time-domain solutions

For a pulsed beam with Gaussian temporal profile of width $1/e$ equal to $\tau_p/2$, $\theta(t)=\left(2/\tau_p\sqrt{\pi}\right)e^{-\left(2t/\tau_p\right)^2}$, the LIU pressure is given by (see Subsection 2 of the Appendix)

$$P_B(\tau_B)=\sum_{n=0}^{\infty}R^{2n}\left[P_B^{[2n\tau]}(\tau_B)-RP_B^{[(2n+2)\tau]}(\tau_B)\right], \tag{5a}$$

$$P_F(\tau_F)=e^{-\frac{\tau}{\tau_{ac}}}\sum_{n=0}^{\infty}R^{2n}\left[P_F^{[2n\tau]}(\tau_F)-RP_F^{[(2n+2)\tau]}(\tau_F)\right], \tag{5b}$$

where

$$P_B^{[2n\tau]}(\tau_B)=\overline{T}\frac{P_0}{2}e^{-\left(\frac{\tau_p}{4\tau_{ac}}\right)^2}e^{-\frac{\tau_B-\tau_B^{2n}}{\tau_{ac}}}\frac{1}{2}$$
$$\times\left[\operatorname{erf}\left(\frac{\tau_B-\tau_B^{2n}}{\frac{\tau_p}{2}}\right)-\operatorname{erf}\left(\frac{\tau_B-\tau_B^{2n}-\tau}{\frac{\tau_p}{2}}\right)\right], \tag{6a}$$

$$P_B^{[(2n+2)\tau]}(\tau_B)=\overline{T}\frac{P_0}{2}e^{-\left(\frac{\tau_p}{4\tau_{ac}}\right)^2}e^{-\frac{\tau_B-\tau_B^{2n+2}}{\tau_{ac}}}\frac{1}{2}$$
$$\times\left[\operatorname{erf}\left(\frac{\tau_B-\tau_B^{2n+1}}{\frac{\tau_p}{2}}\right)-\operatorname{erf}\left(\frac{\tau_B-\tau_B^{2n+1}-\tau}{\frac{\tau_p}{2}}\right)\right], \tag{6b}$$

$$P_F^{[2n\tau]}(\tau_F)=\overline{T}\frac{P_0}{2}e^{-\left(\frac{\tau_p}{4\tau_{ac}}\right)^2}e^{-\frac{\tau_F-\tau_F^{2n}}{\tau_{ac}}}\frac{1}{2}$$
$$\times\left[\operatorname{erf}\left(\frac{\tau_F-\tau_F^{2n}}{\frac{\tau_p}{2}}\right)-\operatorname{erf}\left(\frac{\tau_F-\tau_F^{2n}-\tau}{\frac{\tau_p}{2}}\right)\right], \tag{6c}$$

$$P_F^{[(2n+2)\tau]}(\tau_F)=\overline{T}\frac{P_0}{2}e^{-\left(\frac{\tau_p}{4\tau_{ac}}\right)^2}e^{-\frac{\tau_F-\tau_F^{2n+2}}{\tau_{ac}}}\frac{1}{2}$$
$$\times\left[\operatorname{erf}\left(\frac{\tau_F-\tau_F^{2n+1}}{\frac{\tau_p}{2}}\right)-\operatorname{erf}\left(\frac{\tau_F-\tau_F^{2n+1}-\tau}{\frac{\tau_p}{2}}\right)\right], \tag{6d}$$

and $\tau_{ac}\equiv 1/\omega_{ac}$ is the characteristic acoustic time of LIU. $\tau_B^{2n}=2n\tau+\tau_p^2/8\tau_{ac}$, $\tau_B^{2n+m}=(2n+m)\tau-\tau_p^2/8\tau_{ac}$, $\tau_F^{2n}=2n\tau-\tau_p^2/8\tau_{ac}$, and $\tau_F^{2n+m}=(2n+m)\tau+\tau_p^2/8\tau_{ac}$ with $m=1,2$.

The total backward and forward pressures, in Eq. (5), are the R^2-weighted sum of the two leading sub-pressures, $P_{X\delta}^{[2n\tau]}(\tau_X)$ and $P_{X\delta}^{[(2n+2)\tau]}(\tau_X)$, given by Eq. (6), each of them is the product of an exponential term with a rectangular function.

III. NUMERICAL AND EXPERIMENTAL APPROACH

A numerical implementation of the mathematical model proposed in Sec. II was performed with the aim of analyzing the photoacoustic response in the case of an aluminum slab (strong optical absorber) immersed in a water medium. Typical values of the physical properties for aluminum (sample, s) and water (fluid, f) were used in the computer program, namely, ultrasound speed $c_s=6.32\times10^3\,\mathrm{m\,s^{-1}}$ and $c_f=1.498\times10^3\,\mathrm{m\,s^{-1}}$; mass density $\rho_s=2.7\times10^3\,\mathrm{kg\,m^{-3}}$ and $\rho_f=1\times10^3\,\mathrm{kg\,m^{-3}}$; optical absorption coefficient $\mu=1.4399\times10^8\,\mathrm{m^{-1}}$; specific heat capacity at constant pressure $C_P=9\times10^2\,\mathrm{J\,kg^{-1}\,K^{-1}}$; and volumetric thermal expansion coefficient $\beta=6.9\times10^{-5}\,\mathrm{K^{-1}}$. Characteristic specific acoustic impedance mismatch between the strong absorbing optical plane sample and its surrounding fluid was significant ($Z_s=1.706\times10^7\,\mathrm{Kg\,m^{-2}\,s^{-1}}$, $Z_f=1.498\times10^6\,\mathrm{Kg\,m^{-2}\,s^{-1}}$).

Experiments were conducted to study forward and backward traveling pressure signals induced by pulsed laser irradiation using the setups shown in Figs. 1(a) and 1(b), respectively. The incidence angle in backward mode was less than 2°. The excitation source was a pulsed Nd:YAG laser coupled to an optical parametric oscillator system tuned in at 715 nm. Laser fluence per pulse was set at $I_0=30\,\mathrm{mJ\,cm^{-2}}$ and a beam spot diameter of 12 mm. The spatial beam profile changes with the propagation distance thus, in the near field, it can be approximated as a flat-top beam, as it was required for the model. The time pulse waveform was of the

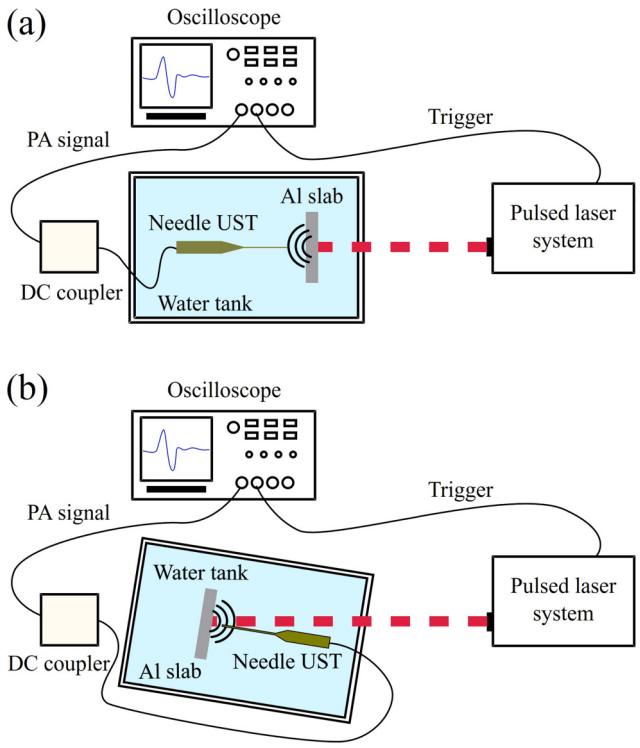

FIG. 1. Experimental setup to generate laser-induced ultrasound in aluminum slabs. (a) Forward and (b) backward modes.

Gaussian type with $\tau_p = 8 \times 10^{-9}$ s and a repetition rate of 10 Hz. 50 mm-diameter metallic slabs were machined from a 99.999% pure aluminum rod with 2.921 mm of thickness. Sample thickness was measured using a Vernier caliper with 1 mil = 25.4 μm resolution. Ultrasound signal was transduced with a 40 μm needle hydrophone having an approximately flat frequency response from 1 to 40 MHz with a ± 4 dB tolerance. A 500 MHz digital oscilloscope was used to acquire the preamplified electrical signal from the needle hydrophone at a sampling rate of 5 GSPS. Trigger signal was provided by the laser control system with an optical pulse jitter < 0.5 ns. Signal treatment processing applied to the delivered waveform consisted in averaging 32 consecutive measurements in order to reduce random or uncorrelated noise. Then, fast Fourier transform (FFT) was performed to the averaged time-domain ultrasound signals. Finally, the zero-padding method was applied with the aim of obtaining a resolution increment in the Fourier power spectrum to 20 kHz. It is essential to highlight that the combined features of the sample and laser pulses fulfilled the long pulse definition ($\mu c \tau_p \approx 7 \times 10^3 \gg 1$).

IV. RESULTS AND DISCUSSIONS

In Eq. (6), error functions difference behave as a continuous rectangular function (a quasi-rectangular function). Equations (A7) and (6) have the same structure: they are the product of an exponential term and a rectangular (or quasi-rectangular) one. The exponential terms represent the electromagnetic-to-mechanical energy conversion, with a rise in time $\tau_{ac} = 1/\omega_{ac}$ (related to the illuminated sample region). While the rectangle, or quasi-rectangle, functions could be interpreted as the space-temporal confinement of this energy. Since the rise time for the rectangle function is equal to zero, a perfect coupling between energy conversion and confinement functions is always achieved for the LIU impulse response, the stress confinement does not matter. Equations (5) and (6) give the time-domain representations for a finite-Gaussian pulse. In these equations, the rise time for the quasi-rectangular continuous functions is equal to $\tau_p/2$, and, then, just for energy conversion rise times compared to this, the coupling occurs.

Figure 2 shows a backward and forward frequency-spectra ($f = \omega/2\pi$), for an aluminum slab with thickness $L = 2.921$ mm. Graphs on Fig. 2(a) were made, from 0 to 50 MHz, by a numerical implementation of Eq. (4). Figure 2(b) is the electrical-signal spectra obtained experimentally. In these figures, black and red lines are for backward and forward signals, respectively. Even though these should not be compared directly, they share some generic structure and a description can be made. First, both LIU signals are complementary, the backward always greater than the forward. Second, both signals show a periodic channeled structure, where sharp minima in backward mode coincided with sharp maxima in the forward mode. This behavior is a consequence of reflections inside the sample and the asymmetry caused by the illumination. Third, the spectral periodicity of the pattern is $\Delta f = 1/2\tau = c_s/2L$. Fourth, since simulations were made with a Gaussian laser pulse time, the spectrum is limited in bandwidth; theoretically, the cut-off frequency is obtained considering the point where pressure magnitude drops to $1/e$ of the maximum value, being $f_{\text{cut}} = 2/\pi\tau_p \approx 80$ MHz; however, experimentally it is bounded by the sensor response-bandwidth. The bandwidth for the δ-pulse spectra is in the order of GHz. Finally, it was observed that the experimental spectra-amplitudes are strongly influenced by the position of the sensor (data not shown); however, the channeled structure remains.

Figures 3(a) and 3(b) show the backward and forward signals, respectively, obtained numerically from Eqs. (A6) and (A7) for $n = 0$. Here, one can see the exponential behavior inherited from the electromagnetic-to-mechanical energy conversion function. In Fig. 3(c), the normalized backward (black lines) and forward (red lines) impulse-response signals are compared with the experimental ones in Fig. 3(d). In both cases (numerical and experimental), the signals consist of the main pressure peak, followed by retarded and inverted reflections at $\tau_B = 2n\tau$ for backward signals and $\tau_F = (2n+1)\tau$ for the forward ones. Even though the confinement stress is not fulfilled, the theoretical reflection times of flight are in agreement with the experimental ones. Discrepancies between the pressure amplitudes and electrical signals, in frequency and time domain, are because the transducer impulse response (in the time domain) and transfer function (in the frequency domain) effects on LIU signal have not been considered yet.

For strongly optically absorbent samples, like metals, the theoretical predicted LIU waves are equal to zero, while the experimental LIU amplitude is different to zero (see Fig. 3). To see this fact, we will analyze the non-reflected backward signals for $n = 0$ [see Eqs. (5a) and (6a)], this analysis can be applied to any other signal

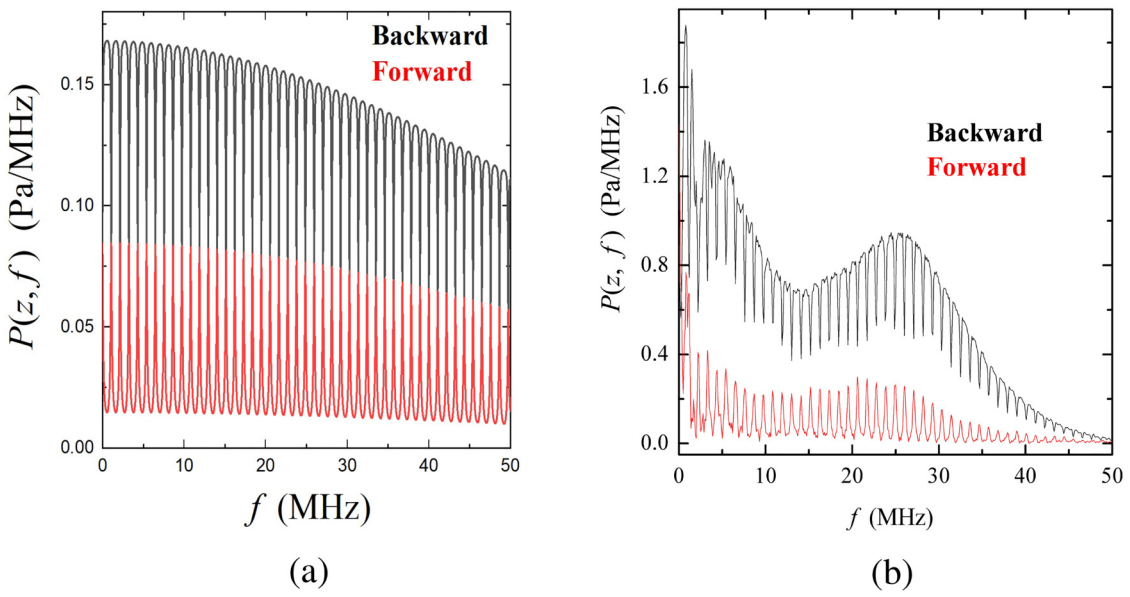

FIG. 2. Comparison between (a) numerical and (b) experimental results in the frequency domain.

and for any n. The non-reflected backward LIU pressure can be written as $P_B^{[0]\tau} = \bar{T}\frac{P_0}{2}F_1(\tau_B)\cdot F_2(\tau_B)$, where

$$F_1(\tau_B) \equiv e^{\left[\frac{\tau_B}{\tau_{ac}} - \left(\frac{\tau_p}{4\tau_{ac}}\right)^2\right]}$$

and

$$F_2(\tau_B) \equiv \frac{1}{2}\left\{\operatorname{erf}\left[\frac{2\tau_{ac}}{\tau_p}\left[\frac{\tau_B}{\tau_{ac}} - 2\left(\frac{\tau_p}{4\tau_{ac}}\right)^2\right]\right] - \operatorname{erf}\left[\frac{2\tau_{ac}}{\tau_p}\left[\frac{\tau_B}{\tau_{ac}} - 2\left(\frac{\tau_p}{4\tau_{ac}}\right)^2 - \frac{\tau}{\tau_{ac}}\right]\right]\right\}.$$

$F_1(\tau_B)$ is monotonically decreasing ranged $e^{-m} < F_1(\tau_B) < e^{+\left(\frac{\tau_p}{4\tau_{ac}}\right)^2}$ in the interval $\tau_{1B} < \tau_B < \tau_{2B}$, where $\tau_{1B} = 0$, $\tau_{2B} = \tau_{ac}\left[m + \left(\frac{\tau_p}{4\tau_{ac}}\right)^2\right]$, and $m \in \mathbb{N}$. Then,

$$F_2(\tau_{1B}) = \frac{1}{2}\left\{-\operatorname{erf}\left[\frac{\tau_p}{4\tau_{ac}}\right] + \operatorname{erf}\left[\frac{\tau_p}{4\tau_{ac}} + \frac{\tau}{\tau_{ac}}\right]\right\}.$$

Since $\tau_p/4\tau_{ac} \approx 1.8 \times 10^3 \gg 2$, the error functions are equal to 1, and $F_2(0) = 0$. On the other hand,

$$F_2(\tau_{2B}) = \frac{1}{2}\left\{\operatorname{erf}\left[\frac{2\tau_{ac}}{\tau_p}\left[m - \left(\frac{\tau_p}{4\tau_{ac}}\right)^2\right]\right] - \operatorname{erf}\left[\frac{2\tau_{ac}}{\tau_p}\left[m - \left(\frac{\tau_p}{4\tau_{ac}}\right)^2 - \frac{\tau}{\tau_{ac}}\right]\right]\right\}.$$

In this case, the error functions are different to 1 if the arguments are close to zero, this implies that $m \approx 10^6$. Then, for the uncorrected solutions, when $F_1(\tau_B)$ is different to zero, $F_2(\tau_B)$ is equal to zero and vice versa.

Even though the energy transformation process from optical to thermal is a very fast phenomenon, heat travels a distance larger than $1/\mu$ during the time where pulse laser is turned on. An approach to overcome this contradiction could be solving analytically the coupled Eqs. (1) and (2) in 1D. However, this is a very hard task and, consequently, a numerical solution is proposed. In order to have a solution for this problem, the next hypothesis is considered: *It is assumed that during the time τ_p, heat travels a characteristic thermal length $l_{\text{th}} = 4\sqrt{\chi\tau_p}$, in consequence, the effective LIU source (thermal source) is $l_{\text{eff}} = 4\sqrt{\chi\tau_p} + 1/\mu$ (thermal plus optical source), then the characteristic acoustic time become*

$$\tau_{ac} \to \tau_{\text{eff}} \equiv \frac{l_{\text{eff}}}{c_s} = \left(1 + 4\mu\sqrt{\chi\tau_p}\right)\tau_{ac}.$$

Due to the relation between τ_{ac} and ω_{ac}, the proposed hypothesis of the use of τ_{eff} instead of τ_{ac} implies the use of $\omega_{\text{eff}} = 1/\tau_{\text{eff}}$ instead of ω_{ac}.

By taking into account the aluminum slab with $\chi = 9.7 \times 10^{-5}$ m^2/s, τ_{eff} is ~0.25 times $\tau_p/2$ and the LIU pressure becomes different to zero; this is shown in Figs. 4(a) and 4(b) for the time and frequency spectra, respectively.

In comparison with the impulse-response signals, the numerical amplitudes of this thermally corrected solution are attenuated, and this is an effect of the finite time pulse and the corrected PA source. More precisely, each laser pulse generates two waves inside the sample; one of them travels to the left and the other one to the

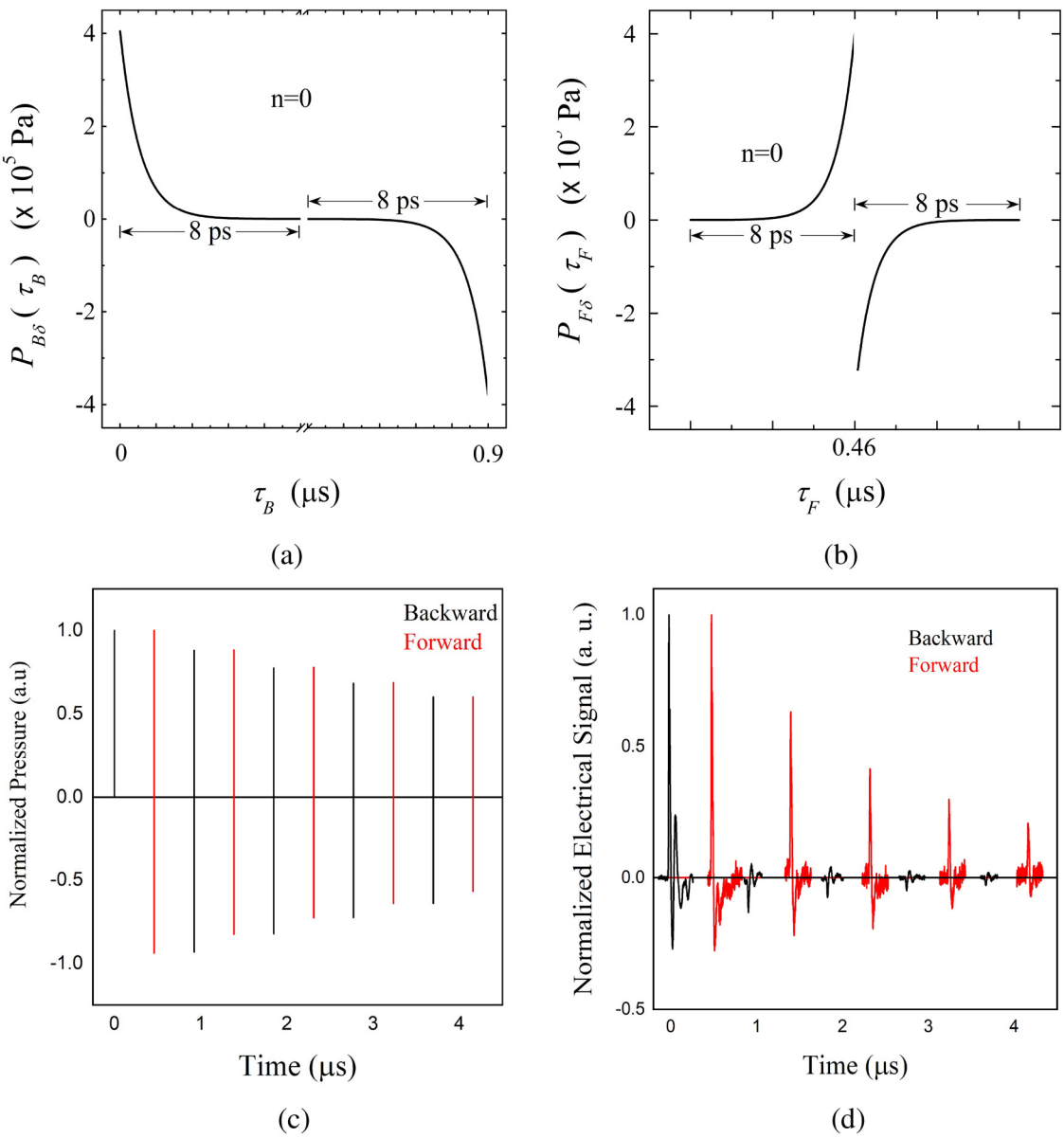

FIG. 3. Simulated time-domain PA signal using Eqs. (A6a) and (A6b). (a) and (b) Backward and forward propagated mode, respectively, for n=0. Here, it can be seen that the solution for the impulse response is discontinuous. (c) Comparison between forward and backward solutions using Eq. (A6) for $n = 5$ and (d) comparison between forward and backward electrical signals.

right. A fraction of the left-wave is transmitted and the other one is reflected in the sample's left-face. Then, the left-reflected wave interferes partially with the original right-wave, and it is reflected on the sample's right-face, leaving the sample. Theoretically, this process is repeated up to infinity; in the experiments, just the first five reflections are observable. Moreover, both the impulse response (delta temporal profile) and this approximation (thermally corrected PA source) agree with the electrical signal times of flight. Additionally, the corrected numerical amplitude widths are thinner than the experimental ones, and these last have more structure. It is paramount to highlight that the attenuation of the reflections does not follow the theoretical predictions $Tp_0R^{2n}/2$ and $-Tp_0R^{2n+1}/2$. All these are because the LIU amplitude is affected by the sensor bandwidth, reflections inside of it, and the effect of the finite

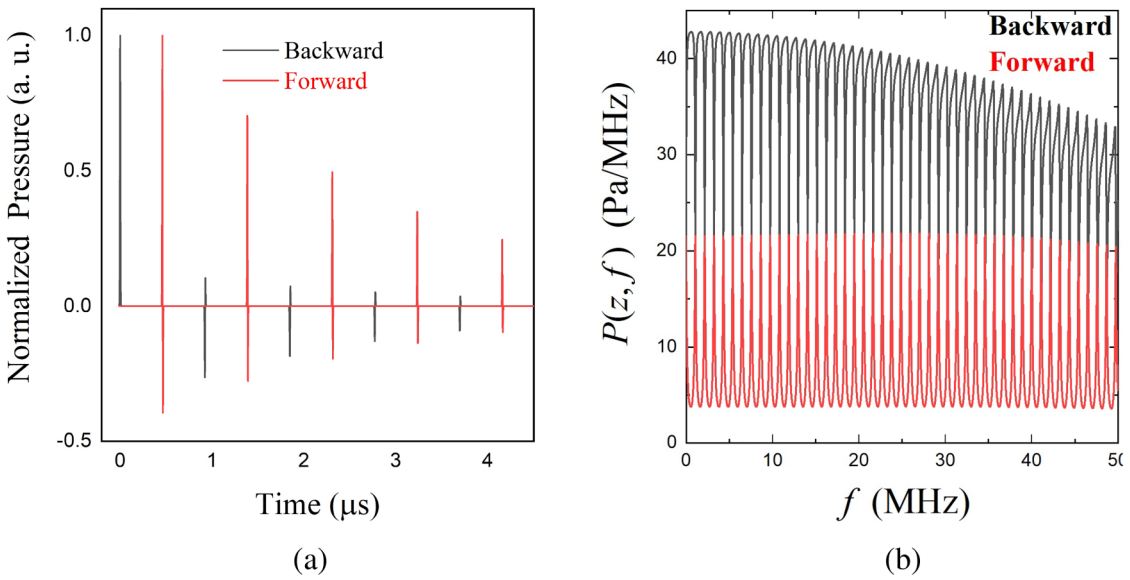

FIG. 4. Thermally corrected LIU pressure in (a) time and (b) frequency domain using ω_{eff} in Eq. (4) and τ_{eff} in Eq. (5).

temporal pulse. The correction effect in the frequency domain was in the channeled structure of the amplitudes, smoothing the curvature of channels.

To better compare both LIU signals obtained through the theoretical model and the implemented experiment, it is necessary to consider the sensor response. The LIU pressure generates a charge in the piezoelectric that flows from it to the oscilloscope along a cable, the electrical circuit that exemplifies this is a parallel RC circuit, with a time-varying input source of charge $Q_0(t)$, an electrical resistance R_e, a capacitance C, and an electric potential difference $U(t)$ (see Fig. 5). For such an electrical circuit, the differential equation for the charge is $R_e C\dot{Q}(t) + Q(t) = Q_0(t)$, with

$$Q_0(t) = \frac{e_{33}A}{d}\int_0^d P(z,t)dz = e_{33}A\overline{P}(t), \tag{7}$$

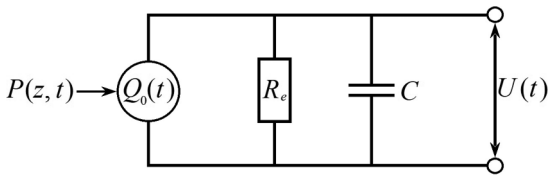

FIG. 5. Equivalent electrical circuit of a hydrophone that generates a charge Q_0, connected through a cable to an oscilloscope of input impedance dependent on a resistance R_e and a capacitance C.

where A is the active area of the transducer, e_{33} is the piezoelectric stress constant, d is the thickness of the foil, and $\overline{P}(t)$ is the mean stress inside it.[19] In order to obtain a solution to the differential equation and derive an expression to the electric potential difference detected by the oscilloscope and generated by the LIU pressure, the transfer function of the RC circuit in parallel was calculated from the differential equation, getting

$$\hat{F}(\omega) = \frac{e_{33}A}{\sqrt{2\pi}}\frac{1}{1+j\omega R_e C}. \tag{8}$$

Then, in the frequency domain, the solution to the differential equation for the charge can be written as $\hat{Q}(\omega) = \hat{F}(\omega)\overline{P}(\omega)$.[20]

The spatial mean values of the backward and forward LIU pressure can be calculated considering a detection position z_X and integrating $\hat{P}_B$ and $\hat{P}_F$ over the piezoelectric thickness d, obtaining

$$\begin{aligned}\overline{P}_X(z_X,\omega) &= \frac{1}{j\omega t_d}\left[\hat{P}_X(z_X - d,\omega) - \hat{P}_X(z_X,\omega)\right]\\ &= \frac{1}{j\omega t_d}\left(1 - e^{-j\omega t_d}\right)\hat{P}_X(z_X,\omega),\end{aligned} \tag{9}$$

where $X = B$ (backward) or F (forward), $t_d = d/c_{piezo}$, c_{piezo} is the sound speed in the piezoelectric, z_X is the position where the LIU wave impinges the sensor, and P_X is given by Eq. (4a) for $X = B$ and (4b) for $X = F$. Since the potential difference is given by $\hat{U}(\omega) = j\omega R_e\hat{Q}(\omega)$, then from Eqs. (5a) and (5b) in the time

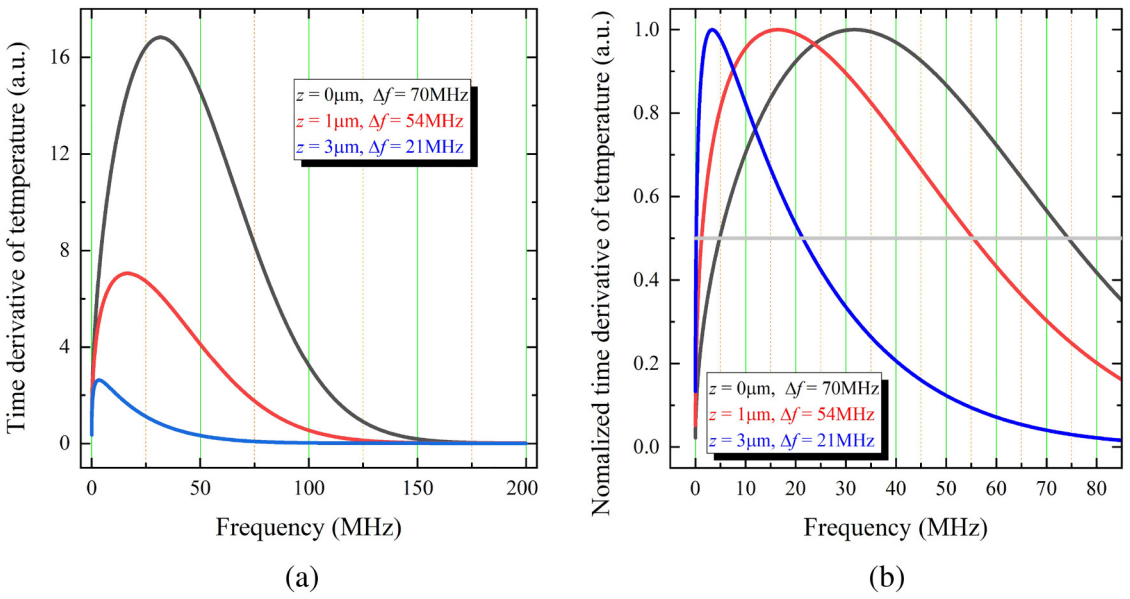

FIG. 6. (a) Time derivative and (b) normalized time derivative of the temperature for different values of its penetration through the sample.

domain, $U_x(t)$ can be now expressed as

$$U_x(t) = \frac{R_e}{t_d} I(t) * [P_x(\tau_x - t_d) - P_x(\tau_x)],$$

where $I(t)$ is the sensor's impulse response, * is the convolution operation, and P_x are given by Eqs. (5) and (6). If the RC electric circuit has a low impedance so that $\omega R_e C \ll 1$, Eq. (8) can be approximated to $e_{33}A/\sqrt{2\pi}$, then $I(t) \approx \delta(t)$ and the electrical signal in the time domain is

$$U_x(t) \approx \frac{R_e}{t_d} [P_x(\tau_x - t_d) - P_x(\tau_x)]. \tag{10}$$

In Fig. 7, a comparison, both in frequency and in the time domains, between the experimental and numerically generated electrical signals is shown. Here, it was assumed that the thickness and the sound speed of the sensor are 100 μm and 2.2×10^3 m/s, respectively. As can be seen in Figs. 7(a) and 7(b), the sensor model generates a signal modulated by their thickness and sound speed, the first wave train being the one that closely match with the experimental electrical signal. On the other hand, the low coincidence and the fast attenuation from the experimental signals could be understood by following the next three aspects: first, the integrated circuit amplifying the electrical signal is not considered in the model. Second, by solving the 1D-heat diffusion with Cauchy boundary conditions for the geometry shown in Fig. 8 [considering that in the left (right)-side there is only thermal wave traveling to the left(right)], a numerical calculation of the temperature derivative was done. In the solution, it was considered that the thermal source is generated by Gaussian pulse with the same parameters used in the wave equation, and it is shown that the temperature derivative spectra reduce its bandwidth three times after traveling 3 μm through the sample (see Fig. 6). As a consequence of this, in the time domain, the temperature-pulse width must increase. If this is taken into account, the second and third train waves [see insets in Figs. 7(a) and 7(b)] are comparable to the experimental signals. However, if these changes are made in the time domain calculations, the LIU amplitudes vanish. Third, the theoretical spectrum is the exact Fourier transform while the experimental one is obtained by the FFT method. It is well known that the FFT method has a loss of information.

In Figs. 7(c) and 7(d), the normalized LIU amplitudes are shown in the time domain. In the insets, the first peaks are displayed for both forward and backward LIU waves. Several aspects must be mentioned. Due to amplitude differences, the peak of the numerical solution at $t = 0$ is now bipolar, as observed experimentally. This shows that the sensor generates, by the difference of the signals, the second peak at $t = 0$. However, because the width of these peaks is narrow, it does not interfere and the negative peak is bigger than the experimental, and this can be seen in the inset of Fig. 7(c). Second, the theoretical amplitudes of backward waves, for $t > 0$, has a different and more complex structure, and this is due to the acoustic wave reflections inside the sensor material. Third, even though the width of the theoretical signals is not well defined, the width of the experimental peaks is explained by the difference of the acoustical signals due to the sensor. The shape of the forward waves can be explained in the same way.

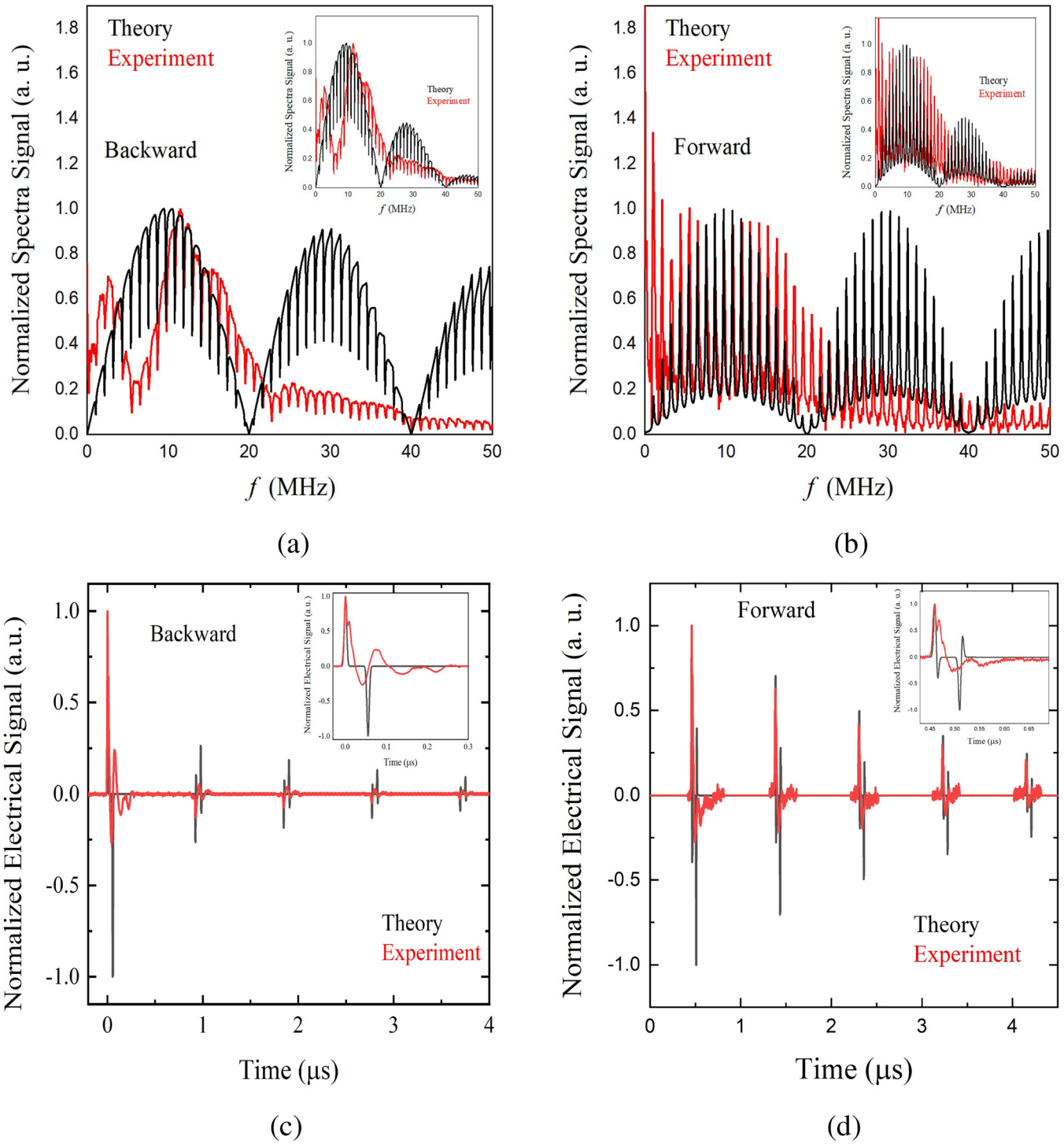

FIG. 7. For the (a) backward and (b) forward propagated mode, comparison between experimental and numerical results in the frequency domain using Eq. (9); in insets, the frequency spectrum is shown when the temperature-pulse width is increased. (c) and (d) Comparison between experimental and numerical results in the time domain using Eq. (10) for the backward and forward propagated mode, respectively; the first peak of both experimental and numerical results are displayed in insets.

Finally, another possible source of discrepancies between our model and the experiments is the heat diffusion from the sample to the fluid.

V. CONCLUSIONS

In this paper, it was shown that by considering the thermal correction for the acoustic source, the 1-D wave equation may be a valid approximation for the generation and propagation of LIU in solid samples with strong optical absorption properties. Previous studies have reported that this approach is good for soft matter and for low optical absorption materials; then, it could be a good approximation to describe the LIU for a broad range of materials.

It is proposed that the photoacoustic source is not only the optical absorption region but also the region where the temperature has increased, leading to a redefinition of the thermal confinement condition that is valid for both weakly and strongly optically absorbent samples. Besides, it was shown that the thermal correction implies that the thermal confinement condition must be $1 \gg 4\mu\sqrt{\chi\tau_p}$, which is in perfect concordance with that defined in the literature. In addition, by considering the thermal correction for the ultrasound source, it is possible to redefine the stress confinement condition as follows: $\left(1 + 4\mu\sqrt{\chi\tau_p}\right)\tau_{ac} \gg \tau_p$.

To better compare the corrected-theoretical results with the electrical signals measured, the sensor and the oscilloscope were modeled as a parallel RC electrical circuit. It was found that the electrical signals were proportional to the difference of the LIU amplitudes at the faces of the sensor. Although the sensor impulse response was modeled as a Dirac delta distribution, this difference strongly affects the shape of the LIU electrical signals, hiding relevant information of the acoustic waves.

ACKNOWLEDGMENTS

This research was partially supported by the Consejo Nacional de Ciencia y Tecnología-México (Fronteras de la Ciencia Grant Nos. FC2029 and FC612-1) and the Dirección de Apoyo a la Investigación y el Posgrado (DAIP) de la Universidad de Guanajuato (CIIC Grant No. 341/2019). We thank Dr. Arturo González-Vega from the Universidad de Guanajuato at León and Dr. Crescencio García-Segundo from the UNAM for their important comments.

APPENDIX: 1D-WAVE EQUATION PROBLEM STATEMENT

For a plane sample s, with thickness L, immerse on a non-optically absorbent fluid f (see Fig. 8), the 1D PA boundary value problem is defined by the following differential equations:[17]

$$\left(\frac{\partial^2}{\partial z^2} - \frac{1}{c_f^2}\frac{\partial^2}{\partial t^2}\right)P_B(z,t) = 0, \quad z < 0, \tag{A1a}$$

$$\left(\frac{\partial^2}{\partial z^2} - \frac{1}{c_s^2}\frac{\partial^2}{\partial t^2}\right)P_s(z,t) = -\frac{\beta}{C_p}\frac{\partial H(z,t)}{\partial t}, \quad 0 < z < L, \tag{A1b}$$

$$\left(\frac{\partial^2}{\partial z^2} - \frac{1}{c_f^2}\frac{\partial^2}{\partial t^2}\right)P_F(z,t) = 0, \quad L < z, \tag{A1c}$$

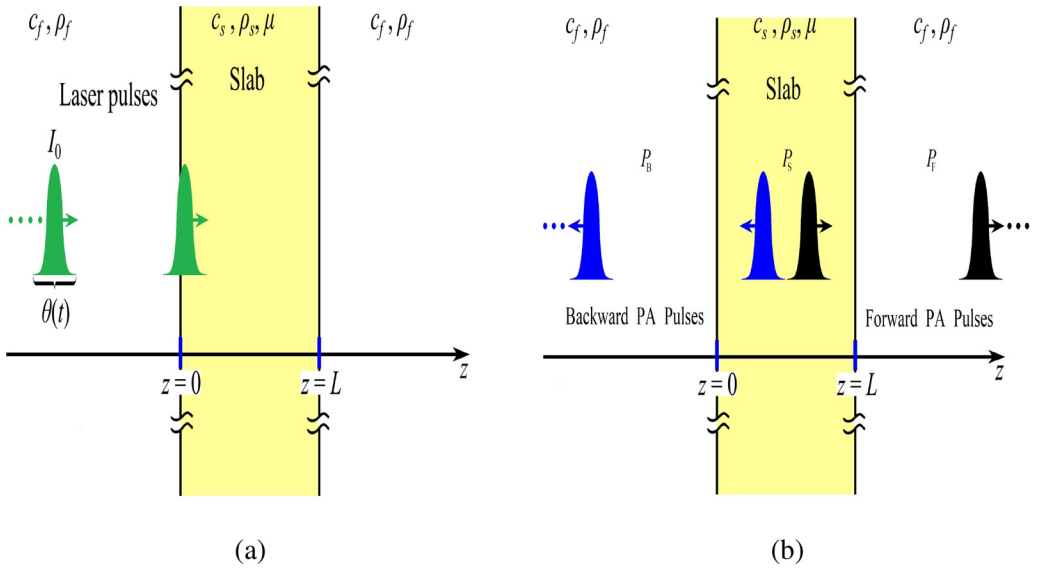

FIG. 8. Schematic representation of the physical photoacoustic model. (a) Representation of the light absorption process and (b) generation of the backward (blue) and forward (black) waves.

coupled with the boundary conditions

$$P_B(z,t)\big|_{z=0} = P_s(z,t)big|_{z=0}, \tag{A2a}$$

$$P_s(z,t)\big|_{z=L} = P_F(z,t)\big|_{z=L}, \tag{A2b}$$

$$\frac{1}{\rho_f}\frac{\partial}{\partial z}P_B(z,t)\bigg|_{z=0} = \frac{1}{\rho_s}\frac{\partial}{\partial z}P_s(z,t)\bigg|_{z=0}, \tag{A2c}$$

$$\frac{1}{\rho_s}\frac{\partial}{\partial z}P_s(z,t)\bigg|_{z=L} = \frac{1}{\rho_f}\frac{\partial}{\partial z}P_F(z,t)\bigg|_{z=L}, \tag{A2d}$$

where subindexes B and F indicate the backward and forward propagated pressures, respectively, while s indicates the pressure field inside the sample.

1. Frequency domain solution

Differential equation solutions for the spatial part of Eq. (A1) are written, after Fourier transforming the temporal part, as[17]

$$\hat{P}_B(z,\omega) = A_B(\omega)e^{j\omega z/c_f} + B_B(\omega)e^{-j\omega z/c_f}, \quad z<0, \tag{A3a}$$

$$\hat{P}_s(z,\omega) = A_s(\omega)e^{j\omega z/c_S} + B_s(\omega)e^{-j\omega z/c_S} + \hat{P}_p(z,\omega), \quad 0<z<L, \tag{A3b}$$

$$\hat{P}_F(z,\omega) = A_F(\omega)e^{j\omega z/c_f} + B_F(\omega)e^{-j\omega z/c_f}, \quad L<z, \tag{A3c}$$

where A_k and B_k, with $k=\{B,s,F\}$, are ω-dependent functions to be obtained from the boundary conditions. The Fourier transform of the particular solution of the inhomogeneous Eq. (A1b) is expressed as

$$\hat{P}_p(z,\omega) = -jP_0e^{-\mu z}\frac{\omega\hat{\theta}(\omega)}{c_s^2\mu^2+\omega^2},$$

where $P_0=\Gamma\mu I_0$, $\Gamma\equiv c_s^2\beta/C_p$ is the Grüneisen parameter, and $\hat{\theta}(\omega)$ is the Fourier transform of $\theta(t)$. Since there are no sources into the fluid, there are only PA waves traveling away from the sample ends; thus, for $z<0$, the LIU signal is a left-traveling wave, and for $z>L$, another pressure wave is propagating to the right. In consequence, B_B and A_F coefficients are equal to zero. To determine the remaining constant coefficients in (A3), boundary conditions in (A2) are Fourier transformed. After solving the system, the frequency dependent functions A_B, A_s, B_s, and B_F were found as

$$A_B(\omega) = \overline{T}\frac{P_0}{2}\left(\frac{\bar{Y}-RYe^{-2j\omega\tau}}{1-R^2e^{-2j\omega\tau}}\right)\hat{\theta}(\omega), \tag{A4a}$$

$$A_s(\omega) = \frac{P_0}{2}\left[\frac{j}{\omega-j\omega_{ac}} + \left(\frac{\bar{Y}-RYe^{-2j\omega\tau}}{1-R^2e^{-2j\omega\tau}}\right)\right]\hat{\theta}(\omega), \tag{A4b}$$

$$B_s(\omega) = \frac{P_0}{2}\left[\frac{j}{\omega+j\omega_{ac}} - \left(\frac{\bar{Y}-RYe^{-2j\omega\tau}}{1-R^2e^{-2j\omega\tau}}\right)R\right]\hat{\theta}(\omega), \tag{A4c}$$

$$B_F(\omega) = \overline{T}\frac{P_0}{2}\left(\frac{Y-R\bar{Y}}{1-R^2e^{-2j\omega\tau}}\right)e^{-jk_f\left[c_f\tau-L\right]}\hat{\theta}(\omega), \tag{A4d}$$

where $\tau=L/c_s$ is the single-trip time-of-flight of the acoustic wave in the slab and $\omega_{ac}\equiv\mu c_s$ is the characteristic ultrasonic frequency of LIU. $R\equiv\left(Z_s-Z_f\right)/\left(Z_s+Z_f\right)$ is the acoustic reflectivity for fluid and sample $\left(\overline{T}=1-R\right)$, where $Z_l\equiv c_l\rho_l$ with $l=\{f,s\}$ for fluid and sample respectively. $Y\equiv\left[1-e^{-(\omega_{ac}-j\omega)\tau}\right]/(\omega_{ac}-j\omega)$ and $\bar{Y}$ the complex conjugate of Y.

Since LIU is a non-contact technique, phenomenological experimentally measurable variables are given by (A4a) and (A4d). Due to the mathematical equality $\left(1-R^2e^{-j2\omega\tau}\right)^{-1} = \sum_{n=0}^{\infty}R^{2n}e^{-j2n\omega\tau}$, the relationships given by these pressures are given by Eq. (4).

2. Time-domain solutions

The time-domain impulse response for pressure is obtained after a time inverse Fourier transformation of Eq. (4) with $\hat{\theta}(\omega)=1/\sqrt{2\pi}$, resulting in

$$P_{X\delta}(\tau_B) = \sum_{n=0}^{\infty}\left\{P_{X\delta}^{[2n\tau]}(\tau_X) - RP_X^{[(2n+1)\tau]}(\tau_X)\right\}, \tag{A5}$$

with

$$P_{B\delta}(\tau_B) = \sum_{n=0}^{\infty}R^{2n}\left\{P_{B\delta}^{[-2n\tau]}(\tau_B) - Re^{-2\tau/\tau_{ac}}P_B^{[+2n\tau]}(\tau_B)\right\}, \quad z\le 0, \tag{A6a}$$

$$P_{F\delta}(\tau_F) = \sum_{n=0}^{\infty}\left\{P_{F\delta}^{[2n\tau]}(\tau_F) - RP_F^{[(2n+1)\tau]}(\tau_F)\right\}, \quad z\ge L, \tag{A6b}$$

where $X=B$ or F for $z\le 0$ or $z\ge L$, respectively, where

$$P_{B\delta}^{[2n\tau]}(\tau_B) = \overline{T}\frac{P_0}{2}R^{2n}e^{-(\tau_B-2n\tau)/\tau_{ac}}\Pi\left[\frac{\tau_B-\left(2n+\frac{1}{2}\right)\tau}{\tau}\right], \tag{A7a}$$

$$P_{B\delta}^{[(2n+1)\tau]}(\tau_B) = \overline{T}\frac{P_0}{2}R^{2n}e^{[\tau_B-2(n+1)\tau]/\tau_{ac}}\Pi\left[\frac{\tau_B-\left[(2n+1)+\frac{1}{2}\right]\tau}{\tau}\right], \tag{A7b}$$

$$P_{F\delta}^{[2n\tau]}(\tau_F) = \overline{T}\frac{P_0}{2}R^{2n}e^{-\tau/\tau_{ac}}e^{(\tau_F-2n\tau)/\tau_{ac}}\Pi\left[\frac{\tau_F-\left(2n+\frac{1}{2}\right)\tau}{\tau}\right], \tag{A7c}$$

$$P_{F\delta}^{[(2n+1)\tau]}(\tau_F) = \overline{T}\frac{P_0}{2}R^{2n}e^{-[\tau_F-(2n+1)\tau]/\tau_{ac}}\Pi\left[\frac{\tau_F-\left((2n+1)+\frac{1}{2}\right)\tau}{\tau}\right], \tag{A7d}$$

with the definitions: $\tau_{ac} \equiv 1/\omega_{ac}$, $\tau_B \equiv t + z/c_f$, $\tau_F \equiv t - (z - L)/c_f$, and

$$\Pi\left[\frac{\tau_{B,F} - \left((2n+m) + \frac{1}{2}\right)\tau}{\tau}\right],$$

with $m = 0, 1$, being the rectangular function centered at $\tau_{B,F} = [(2n+m) + 1/2]\tau$ and width τ.

For any other laser temporal profile, the LIU pressure is given by

$$P_k(\tau_{B,F}) = P_{k\delta} * \theta(\tau_{B,F}) = \int_{-\infty}^{+\infty} \theta(t) P_{k\delta}(\tau_{B,F} - t)\mathrm{d}t,$$

where * is the convolution operation. Thus, for a pulsed beam with Gaussian temporal profile of width 1/e equal to τ_p, $\theta(t) = \left(2/\tau_p\sqrt{\pi}\right)\mathrm{e}^{-\left(2t/\tau_p\right)^2}$, the LIU pressure obtained is given by Eqs. (5) and (6).

DATA AVAILABILITY

The data that support the findings of this study are available from the corresponding author upon reasonable request.

REFERENCES

[1]B. Cox and P. C. Beard, in *Photoacoustic Imaging and Spectroscopy*, edited by L. Wang (CRC Press, 2009), Chap. 3, pp. 25–34.
[2]M. Xu and L. V. Wang, "Photoacoustic imaging in biomedicine," Rev. Sci. Instrum. **77**, 041101 (2006).
[3]L. V. Wang, *Photoacoustic Imaging and Spectroscopy* (CRC Press, 2009).
[4]V. V. Kozhushko and P. Hess, "Laser-induced focused ultrasound for nondestructive testing and evaluation," J. Appl. Phys. **103**, 124902 (2008).
[5]M. Xu and L. V. Wang, "Photoacoustic imaging in biomedicine," Rev. Sci. Instrum. **77**, 041101 (2006).
[6]S. Kothapalli, T. Ma, S. Vaithilingam, O. Oralkan, B. T. Khuri-Yakub, and S. S. Gambhir, "Deep tissue photoacoustic imaging using a miniaturized 2D capacitive micromachined ultrasonic transducer array," IEEE Trans. Biomed. Eng. **59**, 1199–1204 (2012).
[7]S. Sethuraman, J. H. Amirian, S. H. Litovsky, R. W. Smalling, and S. Y. Emelianov, "*Ex vivo* characterization of atherosclerosis using intravascular photoacoustic imaging," Opt. Express. **15**, 16657–16666 (2007).
[8]J. L. Su, A. B. Karpiouk, B. Wang, and S. Emelianov, "Photoacoustic imaging of clinical metal needles in tissue," J. Biomed. Opt. **15**, 021309 (2010).
[9]P. M. Morse and K. U. Ingard, *Theoretical Acoustics* (Princeton University Press, 1968), pp. 281–283.
[10]G. J. Diebold, T. Sun, and M. I. Khan, "Photoacoustic monopole radiation in one, two, and three dimensions," Phys. Rev. Lett. **67**, 3384 (1991).
[11]T. Sun and G. J. Diebold, "Generation of ultrasonic waves from a layered photoacoustic source," Nature **355**, 806 (1992).
[12]R. J. Dewhurst, T. Li, and G. Gondek, "Amplitude decay of photoacoustic signals in biological tissue when irradiated by nanosecond laser pulses," Proc. SPIE **6437**, 643723 (2007).
[13]G. Gondek, T. Li, R. Lynch, and R. J. Dewhurst, "Decay of photoacoustic signals from biological tissue irradiated by near infrared laser pulses," J. Biomed. Opt. **11**, 11–11–4 (2006).
[14]A. L. McKenzie, "Physics of thermal processes in laser–tissue interaction," Phys. Med. Biol. **35**, 1175–1210 (1990).
[15]D. Cywiak, M. D. Barreiro-Argüelles, M. Cywiak, A. Landa-Curiel, C. Garcia-Segundo, and G. Gutierrez-Juárez, "A one-dimensional solution of the photoacoustic wave equation and its relationship with optical absorption," Int. J. Thermophys. **34**, 1473–1480 (2013).
[16]S. Park, M. Khan, H. Cheng, and G. Diebold, "Photoacoustic effect in strongly absorbing fluids," Ultrasonics **29**, 63–67 (1991).
[17]J. T.-A. Francisco Herrerías-Azcúe, A. Gonzáles Vega, and G. Gutiérrez-Juárez, "Solution for the photoacoustic wave equation with a single spatial degree of freedom, Beer's law absorption of radiation and mechanical barriers," Mod. Phys. Lett. B **27**, 1350135 (2013).
[18]N. Baddour and A. Mandelis, "The effect of acoustic impedance on subsurface absorber geometry reconstruction using 1D frequency-domain photoacoustics," Photoacoustics **3**, 132–142 (2015).
[19]H. Schoeffmann, H. Schmidt-Kloiber, and E. Reichel, "Time-resolved investigations of laser-induced shock waves in water by use of polyvinylidenefluoride hydrophones," J. Appl. Phys. **63**, 46–51 (1988).
[20]C. A. Bravo-Miranda, A. González-Vega, and G. Gutiérrez-Juárez, "Influence of the size, geometry and temporal response of the finite piezoelectric sensor on the photoacoustic signal: The case of the point-like source," Appl. Phys. B **115**, 471–482 (2014).